Diffusion-limited aggregation: Connection to a free-boundary problem and lattice anisotropy

Bayard K. Johnson and Robert F. Sekerka
Department of Physics, Carnegie Mellon University, Pittsburgh, Pennsylvania 15213
(Received 19 June 1995)

We study the relationship of diffusion-limited aggregation (DLA) simulations to the solutions of a free-boundary problem that is used to model crystal growth in two spatial dimensions. The mathematical connection between the DLA hitting probability and the normal derivative to the boundary of a growing aggregate is made with particular attention to the lattice anisotropy that systematically appears. Modifications of the original DLA simulation are considered, and the influence of these modifications on the expected growth shape anisotropy is discussed. We present the results of simple DLA and modified DLA simulations. We use a histogramming technique, similar to that used by Arneodo *et al.* for viscous fingering simulations, to display clearly the preferred growth directions of the various simulations. This gives some indication of the effect of simulation modifications on the growth shape anisotropy. We find that both the multiple-hit simulation with erasing, and the multiple-hit simulation without erasing (sometimes referred to as noise-reduced DLA) actually enhance growth shape anisotropy. We conclude that the DLA-like simulatons do not, in general, provide accurate approximate solutions to the continuum model of crystal growth.

PACS number(s): 68.70.+w, 61.43.Bn, 61.43.Hv, 61.50.Cj

I. INTRODUCTION

The diffusion-limited aggregation (DLA) simulation originally introduced by Witten and Sander (which we hereafter refer to as "simple DLA") has attracted much attention in the literature, both because of its simplicity and because of the variety of growth shapes that it can produce [1,2]. The striking similarity of shapes produced by DLA simulations to shapes produced in viscous fingering [3–10], crystal growth [5,11–13], electrochemical deposition [14–17], and in the growth of bacterial colonies [18–20] is especially compelling. The fractal and ramified figures produced from DLA and DLA-like simulations are interesting for their mathematical properties as well as their resemblance to physical systems [21–26].

Much of the literature is devoted to an analysis of the influence of lattice anisotropy on the shapes produced by DLA simulations [5,11,12,27–30]. In particular, Meakin proposed that mega-DLA clusters (clusters of 4×10^6 particles or more) grown on a square lattice exhibit greater sensitivity to the lattice than smaller clusters, and that they exhibit the same sensitivity to the lattice as much smaller "noise-reduced" DLA clusters [5,27]. This idea raises questions about whether the figures produced by the DLA simulations are truly fractal. It also supports the point of view that *kinetic* anisotropy is operative in the DLA simulations, as Ball and Brady suggest in their discussion about growth paths [28]. Other modifications of DLA simulations have been made in attempts to include surface tension and to affect the anisotropy [6,11–13,28]. Many unanswered questions still exist about the mechanism by which an underlying square lattice influences growth shapes which are produced by these simulations.

When interpreting DLA-like simulations, one can usually take one of two different perspectives. The atomistic perspective, in which one views the random walkers as physical particles, can be taken in order to account for physical processes such as interaction energies of the walkers and biased diffusion [31,32]. The continuum perspective, for which the walkers are mathematical entities used to approximate the solution to continuum equations, can be taken in order to relate the simulated growth shapes to forms such as viscous fingers and snowflakes [3,5,12,13,29]. In this paper, we take the latter perspective and study in detail the relationship between the DLA algorithm and the continuum equations that are believed to describe dynamic growth processes. We also consider how anisotropy may appear in these continuum equations.

We demonstrate that the probability distribution and growth mechanism of a simple DLA simulation lead to a set of equations that describe, *in principle,* the isotropic, quasi-steady-state crystal growth problem with no surface tension. A typical figure produced by the simple DLA simulation is shown in Fig. 1. Modifications of simple DLA will be discussed later.

Connections between probability distributions of random walk and functions used in potential theory have been known for a long time [33]. It is important to distinguish between the behavior of a single random walker and a probability distribution for a randomly walking particle. In this paper, we compare probability distributions to the continuous functions used in potential theory. A probability distribution is a function defined over the domain of all possible outcomes. A statistical ensemble of experiments (in DLA, random walking and sticking events) is necessary to calculate a probability distribution by means of a Monte Carlo simulation. In simple DLA, however, one uses one walker at a time to compute a new crystal shape. Thus, the shape changes in

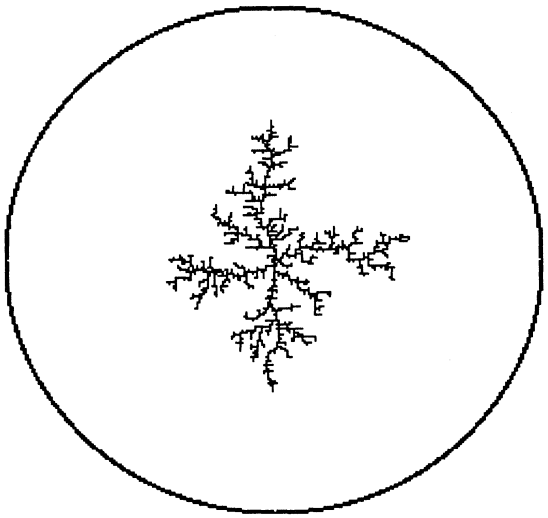

FIG. 1. Typical pattern produced by a diffusion-limited aggregation simulation. Random walkers are released, one at a time, from a circle of radius $150a$, where a is the lattice spacing of the underlying square lattice. The walkers roam on this lattice until they come in contact with the crystal in the center of the circle, at which point they remain for the rest of the simulation. The number of walkers in this figure is 2000. We refer to this simulation as "simple" DLA.

response to an *event,* rather than to a statistical ensemble of events. Although there is this significant distinction between the actual simulation and the results presented here, we believe that the analysis given below will lend some insight into the interpretation of the results of DLA and modified DLA simulations.

The continuous free boundary problem that we seek to make a connection to is crystal growth in the quasi-steady-state approximation (see below) which can be stated as follows: A crystal occupies a region of two-dimensional space (see Fig. 2). This region is surrounded by a large circle of radius R_∞. We can call the region between the crystal and the circle $\tilde{A}$. We define $\delta\tilde{A}^1$ to be the boundary of the crystal, $\delta\tilde{A}^2$ to be the outer boundary of the computational domain at R_∞, and $\delta\tilde{A}\equiv\delta\tilde{A}^1\cup\delta\tilde{A}^2$. In $\tilde{A}$, we calculate the growth potential Φ (which for solidification of a pure material is proportional to the energy density, and for isothermal precipitation is proportional to the concentration) by solving Laplace's equation

$$\nabla^2\Phi=0 \tag{1.1}$$

subject to the Dirichlet boundary conditions

$$\Phi(\mathbf{x})|_{\mathbf{x}\in\delta\tilde{A}}=\overline{\Phi}(\mathbf{x}) , \tag{1.2}$$

where $\overline{\Phi}(\mathbf{x})$ is given on $\mathbf{x}\in\delta\tilde{A}$. We also impose the conservation condition

$$V_N|_{\mathbf{x}_c}=\Gamma\nabla\Phi\cdot\hat{\mathbf{n}}|_{\mathbf{x}_c} , \tag{1.3}$$

where $\mathbf{x}_c\in\delta\tilde{A}^1$, V_N is the normal growth speed of the crystal, $\hat{\mathbf{n}}$ is the unit normal to the crystal at the point $\mathbf{x}_c$ on $\delta\tilde{A}^1$ pointing into $\tilde{A}$, and Γ is a constant that is determined by the diffusivity and other physical parameters. We shall choose $\overline{\Phi}$ on $\delta\tilde{A}^1$ to correspond to conditions that relate to crystal growth. Generally, $\overline{\Phi}$ on $\delta\tilde{A}^2$ is assumed to be constant. If we assume $\overline{\Phi}$ is constant on $\delta\tilde{A}^1$, as we will assume later, the boundary condition (1.2) *does not* include the Gibbs-Thompson effect, according to which Φ at the crystal surface would vary with the curvature.

The only time dependence in this problem is in Eq. (1.3). This problem is therefore the quasi-steady-state (QSS) approximation to the full diffusion problem [34]; this approximation is valid provided that the diffusion field relaxes to its steady-state value in a time that is short compared to that needed for substantial boundary motion. We next proceed to show how a random walk algorithm can be related to solutions to this problem.

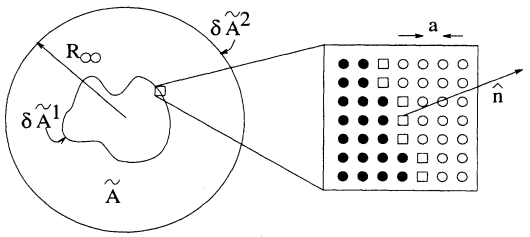

FIG. 2. Computational domain. In a continuum picture, $\tilde{A}$ is the region of the two-dimensional plane between the inner shape and the outer circle shown on the left. Its counterpart, $A=\tilde{A}\cap\mathbb{Z}^2$, in the discrete picture is a subset of the entire discrete two-dimensional square lattice, $\mathbb{Z}^2$, part of which is shown as open circles in the blowup to the right. δA is the set of boundary points of A that are not part of A, and is identified by open squares. The lattice spacing a is much smaller than any length scale in the problem so that the boundary $\delta A=\delta A^1\cup\delta A^2$ is macroscopically smooth.

II. RELATIONSHIP OF SIMPLE DLA TO THE QSS FREE BOUNDARY PROBLEM

In this section we present the basis for the idea that DLA simulations produce shapes which are approximate solutions to the QSS free boundary problem. We first introduce some notation, and then relate random walk to solutions to Laplace's equation with Dirichlet boundary conditions. Finally, we consider the conditions for boundary evolution and see how lattice anisotropy enters.

A. Notation

We begin by introducing some notation that will be used throughout this paper. Much of this notation comes from Spitzer [35]. We denote by $P_n(\mathbf{x},\mathbf{y})$ the probability that after exactly n random jumps on the entire two-dimensional lattice, $\mathbb{Z}^2$, a walker starting from point $\mathbf{x}$ lands on point $\mathbf{y}$ ($\mathbf{x}$ and $\mathbf{y}$ are *vectors* in the plane). The special case for which $n=1$ will simply be denoted $P(\mathbf{x},\mathbf{y})$. We assume that Φ is given for the boundary, δS, of a general set of points, S, that is a subset of $\mathbb{Z}^2$. We assume that the points δS border the set S but *do not* be-

long to the set S. We shall choose the geometry shown in Fig. 2; however, since we study random walk on a square lattice, the set of points A will be the intersection of the set $\bar{A}$ with the integer plane, $\mathbb{Z}^2$, and the set δA will be those points in $\mathbb{Z}^2$ which border A but are not in A. Presently, we consider a general set of points S; later, we will replace S with our specific set of points, A.

One measure of the distance of any point $\mathbf{x}$, in S, from δS is T_S, called the stopping time, which is an integer since it is to be measured in terms of a number of jumps. This is the number of jumps taken by a random walker before its first jump off of the set S. If $\mathbf{x}\in\mathbb{Z}^2-S$, then we define $T_S=0$. Two-dimensional random walk is recurrent, meaning that if we start a random walker at the point $\mathbf{x}$ and allow it to take an infinite number of random jumps on $\mathbb{Z}^2$, the walker will eventually have landed on every site on the lattice. This will occur with probability 1. In other words,

$$\sum_{n=0}^{\infty} P_n(\mathbf{x},\mathbf{y};T_{\mathbb{Z}^2-\mathbf{y}}=n)=1 \text{ for all } \mathbf{x},\mathbf{y}\in\mathbb{Z}^2 .$$

The expression in the sum is the probability that a walker from $\mathbf{x}$ moves onto $\mathbf{y}$ in n jumps on the condition that the nth jump is the first time the walker jumps off the set consisting of the entire integer plane minus the point $\mathbf{y}$ (more simply stated, the first time the walker lands on the point $\mathbf{y}$). We observe that $T_S<\infty$ for any starting point $\mathbf{x}$ in S ($=\mathbb{Z}^2-\mathbf{y}$ above) and any nonempty set of landing sites δS ($=\mathbf{y}$ above). This is not true in three dimensions.

Next, we define several distributions arising from considerations of the two-dimensional random walk. Much of this development can be found in Ref. [35]. In later sections, we will relate these distributions to functions found in potential theory. Let $\mathbf{y}$ be a point on the boundary, δS of S. Then

$$H_S(\mathbf{x},\mathbf{y})=\begin{cases}\sum_{n=1}^{\infty} P_n(\mathbf{x},\mathbf{y};T_S=n) & \text{for } \mathbf{x}\in S\\ \delta_{\mathbf{x},\mathbf{y}} & \text{otherwise},\end{cases}$$

$$\Pi_S(\mathbf{x},\mathbf{y})=\sum_{\mathbf{t}\in S} P(\mathbf{x},\mathbf{t})H_S(\mathbf{t},\mathbf{y}) + \sum_{\mathbf{t}\in\mathbb{Z}^2-S} P(\mathbf{x},\mathbf{t})\delta_{\mathbf{x},\mathbf{y}} \quad \text{for } \mathbf{x}\in(\delta S),$$

where $\delta_{x,y}$ is a Kronecker delta function. $H_S(\mathbf{x},\mathbf{y})$ is the probability that the walker's first step from the set S, starting from the point $\mathbf{x}$, is onto the point $\mathbf{y}$. $\Pi_S(\mathbf{x},\mathbf{y})$ is the probability that a walker's first return to δS, after first stepping onto S from the point $\mathbf{x}$, is at $\mathbf{y}$. When $\mathbf{x}=\mathbf{y}$, one adds to that the probability that the walker does not step onto S at all.

We can express the second central difference form of the Laplacian in terms of the stepping probability as follows:

$$\nabla^2\Phi(\mathbf{x})=\frac{4}{a^2}\left[\left\{\sum_{\mathbf{y}\in\mathbb{Z}^2} P(\mathbf{x},\mathbf{y})\Phi(\mathbf{y})\right\}-\Phi(\mathbf{x})\right], \quad (2.1)$$

where $P(\mathbf{x},\mathbf{y})$ is the stepping probability of the simple random walk on a square lattice of spacing a. *Simple 2D random walk* is defined as follows: $P(\mathbf{x},\mathbf{y})=\frac{1}{4}$ when $\mathbf{y}$ is one of the four nearest neighbors to $\mathbf{x}$, and zero otherwise.

B. Anisotropy of landing and escape probabilities

Some probability distributions of a two-dimensional simple random walk on a square lattice depend on the orientation of the lattice, while others do not. To make this point more clear, we present three examples of probability distributions, one which does not depend on the orientation of the lattice and two that do.

If we assume that a walker that is performing a simple random walk is permitted to wander on the entire square lattice, then the probability that, after a certain number of jumps starting from the point $\mathbf{x}$, the walker is at the point $\mathbf{y}$ depends *only* on the distance $|\mathbf{y}-\mathbf{x}|$ and not on the orientation of the vector $\mathbf{y}-\mathbf{x}$ with respect to the axes of the square lattice. This probability distribution for the random walk on a square lattice is therefore isotropic.

Next, we consider the probability that, on the nth jump, a random walker starting from a fixed distance above a line jumps across the line for the first time onto the site $\mathbf{x}_c$. We compute this probability averaged over the available landing sites just across the line. We consider the *average* probability here, because we wish to use this result when we consider the reverse process in which each site on the train of steps is chosen with equal probability to be the *starting site* of a random walk. Since we are working on a square lattice, we must approximate a line by a train of steps (see Fig. 3). For simplicity, imagine that the train of steps is extremely large, and that there are reflection boundaries erected perpendicular to the train of steps at the ends of the train. Since the random walk is isotropic, the probability that after n jumps a walker lands for the first time on the train of steps within a distance $l/2$ of the site $\mathbf{x}_c$, where l is a fixed length, is independent of the orientation of the lattice. But the density of landing sites in that region does depend on the orientation of the lattice and is given by

$$\rho(\mathbf{x}_c)=\frac{f(\theta)}{a}, \quad (2.2)$$

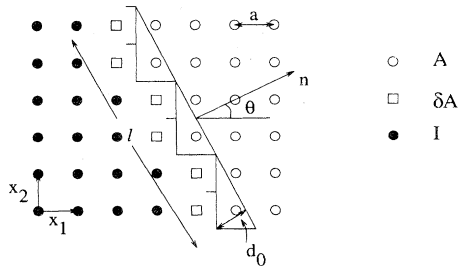

FIG. 3. Sketch of a macroscopically smooth interface of average orientation θ that does not vary over the length l. Growth sites $\mathbf{x}_c$ are in δA. The set $I=\mathbb{Z}^2-(A\cup\delta A)$ are those points that are not in A or δA, and are shown as solid circles; this set constitutes the growing crystal.

where θ is the angle between the normal to the train of steps and the x axis, and where

$$f(\theta)=\frac{1}{\sqrt{2}}\{|\cos(\theta+\pi/4)|+|\sin(\theta+\pi/4)|\} . \quad (2.3)$$

Polar plots of f and $1/f$ are shown in Fig. 4. The probability of landing on the site $\mathbf{x}_c$ is the probability of landing in the region l divided by $(l\rho)$. Stated in terms of an ensemble of walkers: for the same incident flux of walkers, a train of steps which absorbs walkers and which has a low density of landing sites will accumulate more walkers per landing site than one which has a higher density of landing sites. Since the density of landing sites depends on the orientation of the lattice with respect to the absorbing "line," the average probability of landing on a site $\mathbf{x}_c$ will also depend on the orientation of the lattice.

This result can be used to discuss another probability distribution which depends on the orientation of the lattice. Consider the reverse of the process discussed above. Instead of computing the probability that a walker's first visit to a train of steps, starting from a fixed distance above the train of steps, occurs on the nth jump and occurs at the site $\mathbf{x}_c$, we compute the probability that, after n jumps, a walker starting from the site $\mathbf{x}_c$ lands on a train of steps located a fixed distance above the train without ever returning to the train containing $\mathbf{x}_c$. Since each path that a walker can take to accomplish this task can be mapped onto a path for the reverse process with a one-to-one mapping, the probabilities of the two processes are equal. Stated differently, given a fixed number of walkers, starting from a train of steps which absorbs walkers, the flux of walkers across a plane at a fixed distance from the absorbing train depends on the orientation of the lattice with respect to the train. It should be noted that this anisotropy occurs because of the specific rules that we apply at the train of absorbing sites.

The anisotropies discussed above persist even in the limit of very small a. In what follows, we will be careful in our treatment of the probabilities in which these and similar anisotropies appear.

C. Dirichlet potential

We now consider the geometry shown in Fig. 2, and substitute A for the general set S above. For $\mathbf{x}\in A\cup\delta A$, we define the potential

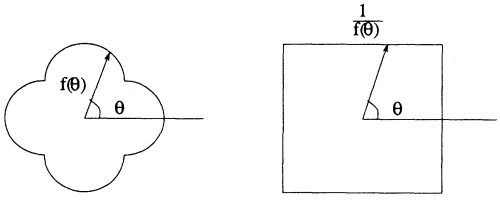

FIG. 4. Polar plot of $f(\theta)$ and $1/f(\theta)$. $f(0)=1.0$. The growth anisotropy induced by growth on a square lattice can be expressed in terms of $f(\theta)$. For simple DLA, this function appears in both the average hitting probability and the average growth speed.

$$\Phi(\mathbf{x})=\sum_{\mathbf{y}\in\delta A} H_A(\mathbf{x},\mathbf{y})\Phi(\mathbf{y}) , \quad (2.4)$$

where $\Phi(\mathbf{y})$ is specified for $\mathbf{y}\in\delta A$ (see Fig. 2). By operating on $\Phi(\mathbf{x})$ with our discrete Laplacian operator, Eq. (2.1), we find that

$$\frac{a^2}{4}\nabla^2\Phi(\mathbf{x})|_{\mathbf{x}\in A}=\sum_{\mathbf{t}\in\mathbb{Z}^2} P(\mathbf{x},\mathbf{t})\left[\sum_{\mathbf{y}\in\delta A} H_A(\mathbf{t},\mathbf{y})\Phi(\mathbf{y})\right] -\Phi(\mathbf{x}) =0 .$$

To see that Φ also satisfies the given boundary conditions for the set A, we notice that $H_A(\mathbf{x},\mathbf{y})$ approaches $\delta_{\mathbf{x},\mathbf{y}}$ when $\mathbf{x}$ approaches δA. Note that Φ on the boundary can vary, provided that the values of Φ for neighboring sites along the boundary do not differ too much. We require this because our expression (2.1) is the result of a Taylor expansion where we have neglected terms of high order in the lattice spacing, a. If Φ varies significantly over distances that are comparable to the lattice spacing, then this approximation is not a good one.

Imagine performing two calculations of Φ for the point $\mathbf{x}$ using Eq. (2.4). In each calculation, we keep the relative positions of our field point, $\mathbf{x}$, and the boundary, δS, fixed, but we approximate the region S by two square lattices that differ in their orientation. Although H_A depends on the relative orientation of the boundary and the lattice near the landing point $\mathbf{y}$, as we discussed in Sec. II B, the number of terms in the sum over sites $\mathbf{y}$ that appear in Eq. (2.4) and that come from the region near $\mathbf{y}$ also depends on the orientation of the lattice near $\mathbf{y}$ in such a way that it cancels the anisotropy from H_A. As a result, $\Phi(\mathbf{x})$ is the same for both cases.

Therefore, if we choose Φ to be defined by Eq. (2.4), Φ will be a discrete approximation to the solution to the Dirichlet boundary value problem in A with value $\Phi(\mathbf{y})$ given for $\mathbf{y}$ on δA and will approach the exact solution in the limit as the lattice spacing approaches zero.

D. Normal derivative

Now that we have found the Dirichlet potential Φ in the region A, we examine the growth condition given by Eq. (1.3). First, as is suggested by Spitzer [35], we consider the function

$$G(\mathbf{x}_c)=\sum_{\mathbf{t}\in A} P(\mathbf{x}_c,\mathbf{t})[\Phi(\mathbf{t})-\Phi(\mathbf{x}_c)] \quad (2.6)$$

for $\mathbf{x}_c\in\delta A^1$, and proceed to relate it to the normal derivative.

If we consider a train of steps representing a portion of the surface of the growth figure that contains the point $\mathbf{x}_c$ and whose normal makes an angle θ with the x axis, we can find expressions for the *average* probabilities $\langle P(\mathbf{x}_c,\mathbf{t})\rangle$ of stepping from δA^1 into A. The brackets $\langle\ \rangle$ represent averages which are taken over a region along δA^1, over which the normal does not vary appreciably, but for which the number of sites is large; denote this subset of δA^1 by $\delta\overline{A}^1$. The average probability of

stepping from sites in $\delta\overline{A}^1$ onto sites in A in one of the possible stepping directions (x or y) can be computed by dividing the number of sites available in that direction by the number of starting sites in the subset $\delta\overline{A}^1$. The average probability of stepping "north" compared to the probability of stepping "east" from one of the surface sites, as shown in Fig. 3, is different and can be written

$$\langle P(\mathbf{x}_c,\mathbf{x}_c+\mathbf{x}_1)\rangle=\frac{1}{4}\frac{l\cos(\theta)}{l\cos(\theta)}=\frac{1}{4}\ ,$$
$$\langle P(\mathbf{x}_c,\mathbf{x}_c+\mathbf{x}_2)\rangle=\frac{1}{4}\frac{l\sin(\theta)}{l\cos(\theta)}=\frac{1}{4}\tan(\theta)\ ,$$

where $\mathbf{x}_1$ and $\mathbf{x}_2$ are vectors of length a pointing in the x and y directions, respectively. These relations hold only for $0<\theta<\pi/4$. We extend these expressions to all possible orientations and compare Eq. (2.6) to the familiar expression for the normal derivative,

$$\frac{\partial\Phi}{\partial\hat{\mathbf{n}}}=\frac{\partial\Phi}{\partial x}\cos(\theta)+\frac{\partial\Phi}{\partial y}\sin(\theta) \tag{2.7}$$

and find

$$\langle G(\mathbf{x}_c)\rangle=\frac{a}{4f(\theta)}\frac{\partial\Phi}{\partial\hat{\mathbf{n}}}\ , \tag{2.8}$$

where we have assumed that derivatives can be replaced by finite differences, and that for $\mathbf{x}$ in the neighborhood, l, of $\mathbf{x}_c$, $\Phi(\mathbf{x}+\mathbf{x}_1)$ and $\Phi(\mathbf{x}+\mathbf{x}_2)$ do not vary with $\mathbf{x}$. The function $f(\theta)$ is the same anisotropy function as given previously by Eq. (2.3) and can be viewed in Fig. 4.

Inserting Eq. (2.4) into (2.6), substituting for $\langle G(\mathbf{x}_x)\rangle$ in (2.8), and using the fact that both P and Π are normalized as follows:

$$\sum_{y\in\delta A}\Pi_A(\mathbf{x}_c,\mathbf{y})=1\ ,$$
$$\sum_{y\in\mathbb{Z}^2}P(\mathbf{x}_c,\mathbf{y})=1\ , \tag{2.9}$$

we find

$$\frac{a}{4f(\theta)}\frac{\partial\Phi}{\partial\hat{\mathbf{n}}}\bigg|_{\mathbf{x}_c}=\left\langle\sum_{\mathbf{y}\in\delta A}\Pi_A(\mathbf{x}_c,\mathbf{y})[\Phi(\mathbf{y})-\Phi(\mathbf{x}_c)]\right\rangle\ . \tag{2.10}$$

We have not yet specified the boundary condition $\Phi(\mathbf{x}_c)$. The expression (2.10) is valid, in general, for any sufficiently smooth domain and smoothly varying Dirichlet boundary condition.

We examine the simple case in which Φ, evaluated on the boundary δA^2, is constant with value Φ_B, and on δA^1 is constant with value Φ_C. Since Φ_C is constant, the terms of the sum in Eq. (2.10) which contain $\Pi_A(\mathbf{x}_c,\mathbf{y})$ for $\mathbf{y}\in\delta A^1$ vanish, and Eq. (2.10) becomes

$$\frac{a}{4f(\theta)}\frac{\partial\Phi}{\partial\hat{\mathbf{n}}}=[\Phi_B-\Phi_C]\left\langle\sum_{\mathbf{y}\in\delta A^2}\Pi_A(\mathbf{x}_c,\mathbf{y})\right\rangle\ . \tag{2.11}$$

We define the DLA hitting probability for the site, $\mathbf{x}_c$, located in δA^1 to be

$$D_1(\mathbf{x}_c)=\sum_{\mathbf{y}\in\delta A^2}h(\mathbf{y})\Pi_A(\mathbf{y},\mathbf{x}_c)$$
$$=\frac{1}{N_B}\sum_{\mathbf{y}\in\delta A^2}\Pi_A(\mathbf{y},\mathbf{x}_c)\ , \tag{2.12}$$

where N_B is the number of starting sites on the outer boundary δA^2, and $h(\mathbf{y})$ is the probability that we choose to start the walker from the site $\mathbf{y}$.

The function $D_1(\mathbf{x}_c)$ is the probability that a walker, starting from a randomly chosen site on the outer boundary, lands on the boundary of the growing figure at the point $\mathbf{x}_c$ before hitting any other sites *in* δA, including sites on the boundary δA^2. The escape probability from sites along the diagonal sections of the outer boundary is larger according to the discussion in Sec. II B. We therefore choose starting sites with a probability that will account for this anisotropy, and produce a probability distribution that is independent of the orientation of the lattice at the points $\mathbf{y}$. This is accomplished by choosing each starting site on the outer boundary with *equal* probability. In some simulations, one chooses starting sites by randomly choosing an angle between 0 and 2π and then starts the walker from the site that is closest to the point on the outer circle that corresponds to that angle. Such an algorithm produces a higher probability for choosing starting sites which are along portions of the circle that are not aligned with the square lattice because each site there covers a larger portion of the circle (the density of sites is lower). By choosing each starting site with equal probability, we have an anisotropic starting probability that just cancels with the anisotropic escape probability, and produces an *isotropic flux* from δA^2. Other significant effects of the absorbing boundary are also discussed by Voss in [36].

By the symmetry of Π_A we conclude that

$$\langle D_1(\mathbf{x}_c)\rangle=\frac{a}{4f(\theta)N_B[\Phi_B-\Phi_C]}\frac{\partial\Phi}{\partial\hat{\mathbf{n}}}\ , \tag{2.13}$$

where we average the DLA hitting probability over a train of steps with orientation θ. This result holds for $\Phi=\Phi_C$ on δA^1, and Φ and Φ_B on δA^2. Note that for a circular crystal and a circular outer boundary, the DLA hitting probability D_1 will be larger for surfaces oriented near the [1,1] direction than for those oriented near the [1,0] direction because of the anisotropic factor $f(\theta)$.

We have tested Eq. (2.13) by means of a simulation. In Fig. 5, we show the dependence of $\langle D_1(\mathbf{x}_c)\rangle$ on the average θ, measured between the normal at $\mathbf{x}_c$ and the x axis, for a simulation in which walkers leave sites that approximate a circle and land on sites that approximate another concentric circle. We actually compute $D_1(\mathbf{x}_c)$ on a wedge between zero and $\pi/4$ with reflection boundary conditions on the sides of the wedge rather than using an entire disk for our computation. This reduction of the computational domain provides us with better statistical accuracy and is justified by symmetry arguments. The actual probability of hitting each site was computed by allowing a large number of walkers to wander from the outer circle and dividing the number that hit sites on the inner circle by the number released. This probability is

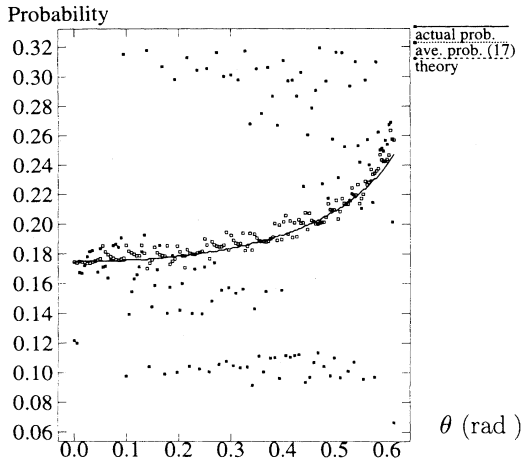

FIG. 5. Plot of the hitting probability, $D_1(\mathbf{x}_c)$, for concentric circles versus the angle between the normal to the surface and the x axis. The computation was done on a pie-shaped region between zero and $\pi/4$. The actual landing probability is plotted with the solid squares. The landing probability varies by about a factor of 3 depending on the local environment of the landing site. The average over 17 neighboring landing sites is plotted with the open squares. This compares well with the predicted probability represented by the solid line.

plotted with solid squares. The probabilities are then averaged over 17 neighboring lattice spaces in each direction; the results are represented by the open squares. We plot Eq. (2.13) with a solid line. This can be computed exactly, because we can compute $\partial\Phi/\partial\hat{\mathbf{n}}$ exactly in this simple geometry. Clearly, there is strong agreement with Eq. (2.13), but there are also large local variations in the hitting probability that we will discuss in Sec. IV.

E. Geometric anisotropy and v_N

If we wish to compute the normal growth speed resulting from adding particles to the surface, we must again consider the surface orientation. Imagine laying one layer of particles on a macroscopically smooth surface whose normal makes an angle θ with the x axis (see Fig. 3). Because the train of N added particles covers the area $\mathcal{A}=Na^2$, and the train spans a length of surface $l=Na/\cos(\theta)$, the average normal growth distance λ for each added particle will be

$$\lambda=\frac{\mathcal{A}}{l}=\frac{Na^2}{Na/\cos(\theta)}=a\cos(\theta)\ .$$

Again, we have only considered the case where $0\le\theta\le\pi/4$. Extending this result to all possible orientations, we conclude that

$$\lambda=\frac{a}{\sqrt{2}}[\,|\cos(\theta+\pi/4)|+|\sin(\theta+\pi/4)|\,]$$
$$=af(\theta)$$

(see Fig. 4).

The normal growth speed v_N is simply the rate of incorporation of particles onto the surface times the normal growth distance per particle. Thus

$$v_N=q\langle D_1(\mathbf{x}_c)\rangle\lambda$$
$$=\frac{qa^2}{4N_B[\Phi_B-\Phi_C]}\frac{\partial\Phi}{\partial\hat{\mathbf{n}}}\bigg|_{\mathbf{x}_c}\ , \tag{2.14}$$

where q is the rate of introduction of particles into the simulation at the outer boundary. The average hitting probability and the average growth distance per particle are anisotropic, but, when one multiplies them, the anisotropic factor $f(\theta)$ cancels, leading to an isotropic growth rate. Thus, *in principle,* the DLA algorithm should solve the free boundary problem described in the Introduction, and the results should be isotropic (they should not be affected by the orientation of the square lattice).

There are two significant discrepancies between this analysis and what one actually does in a DLA simulation. First, the simulation does not, in fact, compute these averages. It uses one random walking event to compute a landing probability, which requires a statistically large number of events, and it does not perform appropriate averaging over neighboring sites. Second, the hitting probability and the growth distance are statistically correlated, so that the product of their averages does not equal the average of their product. We pursue these important points further in the discussion section.

We emphasize that the time dependence in Eq. (2.14) comes solely from the injection rate q of random walkers from the outer boundary. This is also true of the DLA simulation. Much of the literature focuses on the *time-dependent* probability distribution of a random walker, $u(x,t)$, which is the probability that a single walker is at the position $\mathbf{x}$ at time t, and which obeys a discrete version of the diffusion equation. In our opinion, this probability distribution is not of interest in the context of the simple DLA simulation. The probability distributions $D_1(\mathbf{x}_c)$, and the potential $\Phi(\mathbf{x})$ as defined in Eqs. (2.12) and (2.4), respectively, are independent of time, and are the relevant distributions for interpretation of the DLA algorithm. This point is also mentioned in [6].

We found that simple DLA does, in fact, exhibit preferred growth along the x and y axes. Section IV describes a method for observing this preferred growth easily. In Sec. V, we address several questions about the realization of these results in an actual DLA simulation; in particular, we explain how the above considerations do not constitute a complete analysis of the simple DLA simulation.

III. COMPARISON OF TWO-HIT PROBABILITIES

In this section, we discuss a modification of DLA that is similar to the modification referred to as "noise-reduced DLA" in much of the literature [27,5,30,37]. We will refer to the modified version of DLA considered here as multiple-hit DLA with erasing. Multiple-hit DLA with erasing is like simple DLA in that walkers roam on a lattice until they come in contact with the surface of a growth figure, but instead of immediately adding the landing site to the growth figure, one adds unity to a counter at that site. When the counter exceeds a

predetermined value, the site is added to the growth shape and the counters on all other sites are erased. Usually, noise-reduced DLA refers to the algorithm in which counters are not erased after a site has been added. We will hereafter refer to noise-reduced DLA as a multiple-hit DLA without erasing.

Imagine a single growth event occurring on a given configuration (growth figure). The figure will have M available growth sites, each of which can be labeled $m=1,\ldots,M$. Let $D_n(\mathbf{x}_m)$ be the probability that the site labeled $\mathbf{x}_m$ is the first of all M sites to be hit n times. Note that $D_1(\mathbf{x}_m)$ is the simple (one-hit) probability that we defined in Eq. (2.12).

Assume that the single-hit probability of each of these sites is known. We wish to find the two-hit probabilities of sites $\mathbf{x}_1$ and $\mathbf{x}_2$, and to compare them. We can express $D_2(\mathbf{x}_1)$ in terms of $D_1(\mathbf{x}_m)$ for $M=1,\ldots,M$:

$$D_2(\mathbf{x}_1)=D_1(\mathbf{x}_1)D_1(\mathbf{x}_1)+(2!)D_1(\mathbf{x}_1)\left[\sum_{m=2}^{M}D_1(\mathbf{x}_m)\right]D_1(\mathbf{x}_1)$$
$$+(3!)D_1(\mathbf{x}_1)\left[\sum_{3\le n<m\le M}D_1(\mathbf{x}_n)D_1(\mathbf{x}_m)\right]D_1(\mathbf{x}_1)+\cdots . \tag{3.1}$$

The first and second terms on the right hand side are the probabilities that site $\mathbf{x}_1$ is hit twice on the first two trials and the first three trials, respectively. The third term is similarly the probability that the site $\mathbf{x}_1$ is hit twice in the first four trials, but here we had to account for the possibility of another site being hit twice before site $\mathbf{x}_1$ is hit for the second time. This was taken care of by requiring $n\neq m$. The rest of the terms (total of M terms) contain similar sums. If we look closely at the sums that are the coefficients of $[D_1(\mathbf{x}_1)]^2$, we find that they can be factored into two parts: one that has a factor of $D_1(\mathbf{x}_2)$, and another that does not. Therefore, Eq. (3.1) can be simplified by writing

$$D_2(\mathbf{x}_1)=[D_1(\mathbf{x}_1)]^2[KD_1(\mathbf{x}_2)+J] ,$$

where K and J are complicated but positive quantities that do not contain either $D_1(\mathbf{x}_1)$ or $D_1(\mathbf{x}_2)$. Using similar reasoning we can show that

$$D_2(\mathbf{x}_2)=[D_1(\mathbf{x}_2)]^2[KD_1(\mathbf{x}_1)+J] .$$

Here J and K are the *same* values as they are in the expression for $D_2(\mathbf{x}_1)$. We compare $D_2(\mathbf{x}_1)$ and $D_2(\mathbf{x}_2)$ by examining their ratio:

$$\frac{D_2(\mathbf{x}_1)}{D_2(\mathbf{x}_2)}=\frac{[D_1(\mathbf{x}_1)]^2[KD_1(\mathbf{x}_2)+J]}{[D_1(\mathbf{x}_2)]^2[KD_1(\mathbf{x}_1)+J]}$$
$$=\frac{D_1(\mathbf{x}_1)}{D_1(\mathbf{x}_2)}\left[\frac{D_1(\mathbf{x}_1)D_1(\mathbf{x}_2)+(J/K)D_1(\mathbf{x}_1)}{D_1(\mathbf{x}_1)D_1(\mathbf{x}_2)+(J/K)D_1(\mathbf{x}_2)}\right] .$$

We chose to label the M surface sites in an arbitrary way so that site $\mathbf{x}_1$ and site $\mathbf{x}_2$ could be any two sites on the surface. Thus, if $D_1(\mathbf{x}_1)>D_1(\mathbf{x}_2)$, then

$$\left[\frac{D_1(\mathbf{x}_1)}{D_1(\mathbf{x}_2)}\right]^2>\frac{D_2(\mathbf{x}_1)}{D_2(\mathbf{x}_2)}>\frac{D_1(\mathbf{x}_1)}{D_1(\mathbf{x}_2)} . \tag{3.2}$$

Therefore, the growth probabilities of the surface sites will change when we move from one-hit DLA to two-hit DLA. Relative landing probabilities "spread" so that the likely landing sites in single-hit DLA become even more likely, relative to the other sites, when we use two-hit DLA. Also, one can conclude that the spreading of the probabilities is bounded above by $[D_1(\mathbf{x}_1)/D_1(\mathbf{x}_2)]^2$. One can use n-hit DLA with a large n value to raise this upper bound. As we showed in Sec. II, there is a balance between the anisotropy in the hitting probability and that in the normal growth speed. Here, we show that the hitting probability changes when we change from simple DLA to multiple-hit DLA with erasing. We expect this modification to upset the balance between anisotropies, and lead to anisotropic growth shapes.

Two things still must be resolved. First, from our analysis in Sec. II, the spreading of relative growth probabilities would indicate that the preferred growth directions for multiple-hit DLA will be along the diagonals. Our actual simulations, however, indicate that there is preferred growth in the x and y directions. This suggests that the current analysis ignores some important *local* information that might explain the preferred growth along the axes. It may also be also true that the correlations between fluctuations in growth speed and in landing probability are changed in such a way to affect the anisotropy.

Second, we should consider the case of multiple hits in which we *do not* erase the counting on the other sites when we add a particle to a growth site. This analysis will be much more complicated, because we must consider the history of the growth figure. In other words, growth at a given site depends strongly on how recently that site became a surface site. This would have the effect of resisting growth of isolated fingers, as has been pointed out previously [5].

IV. HISTOGRAM

We performed simple DLA and modified DLA simulations to obtain information about the effects of the square lattice on growth shapes. The histogramming method of Arneodo and co-workers was employed to make the effects of the lattice on the anisotropy clear [3,30]. Their method consists of running the simulation to a large number N of times, and recording the sites that are occupied by the crystal for each run. After all of the runs have been completed, one can count the number of times

that each site is a part of the growth shape out of N runs. One can thus obtain a density projection of the likelihood that the growth shape occupies a given region. A similar method was used by Ball and Brady to examine anisotropy in simple and modified DLA simulations [28].

Simple DLA is the simulation first presented by Witten and Sander in Ref. [1]. One releases walkers from the outer boundary and allows them to wander until they hit the surface of the crystal where they immediately become part of the growing cluster. One-slide DLA is the same algorithm as simple DLA, except that when a walker lands on a growth site, one examines the neighboring sites along the interface, and determines if those sites have more solid neighbors than the landing site. If so, then the walker makes a "slide" to the neighboring site with probability 1 and stays there as part of the growing figure. If there is a tie, then one randomly chooses one of the sites, moves the walker there, and allows it to become part of the growing cluster. Two-hit DLA is simply the modified DLA simulation described in Sec. III where new sites are not incorporated into the cluster until two hits have registered. We erase the counting after a new site is added. The two-hit, one-slide version of the simulation is simply one-slide DLA in which one does not incorporate a new site onto the cluster until that site has been the final landing site of walkers, twice. Again we erase the counting on the other sites when a new site is added to the cluster. For comparison, we also perform the two-hit DLA simulations without erasing the counters after a site has been added.

Each histogram represents 100 figures of 1500 particles each. Six different simulations were performed: simple DLA, one slide DLA, two-hit erase DLA, two-hit erase DLA with one slide, two-hit no-erase DLA, and two-hit no-erase DLA with one slide. The results are shown in Figs. 6–8. One can see that the simple DLA simulation 6(a) is not isotropic, but exhibits a preference for growth along the x and y axes. The two-hit simulation 7(a) exhibits a much more dramatic preference for growth along the axes. The one-slide DLA simulation in Fig. 6(b) shows slightly anisotropic growth with preferred growth in the diagonal direction. The two-hit DLA with one slide in Fig. 7(b) exhibits pronounced arms along the diagonal. The slide versions of the simulations are much more compact than the no-slide versions. The two-hit DLA simulations of Fig. 8 in which we do not erase counters also show the enhanced anisotropy that we observe in the "erase" version. Notice that the erase versions of the simulation are much more spread out because growth of the tips is so strongly favored over growth of side arms.

One surprising result is that the one-slide versions of the simulation exhibit a different anisotropic response to the square lattice, compared to the no-slide versions. It has been found [37,38] that the single slide version of the simulation has the same fractal dimension as simple DLA. One might suspect that other aspects of the simulation results will be the same as that of simple DLA, but here we find that the response to the square lattice is completely different. This transition from axial to diagonal growth was also observed by Shonosuke and Honjo

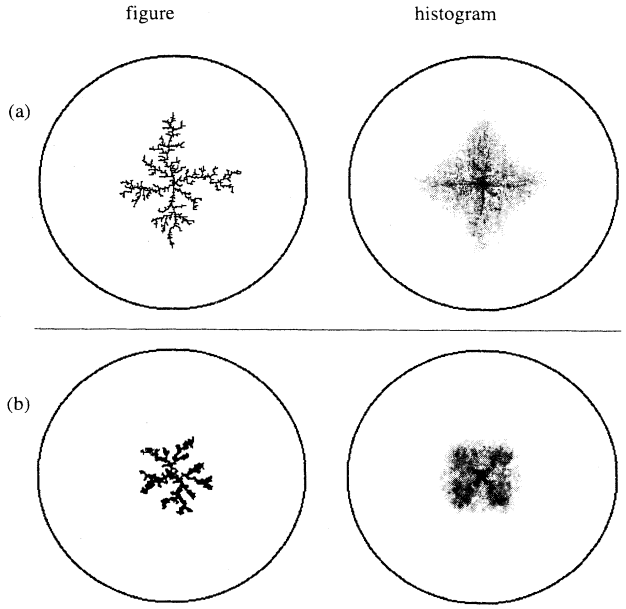

FIG. 6. Results from histogram DLA simulations. The figures on the left are single simulation growth figures of 1500 particles, and the figures on the right are histograms of 100 figures produced by the same algorithm. The shading represents the number of times out of 100 simulations that a growth shape occupied that lattice site. (a) is a simple DLA simulation, and (b) is one-slide DLA. The histograms show a slight anisotropic response to the lattice.

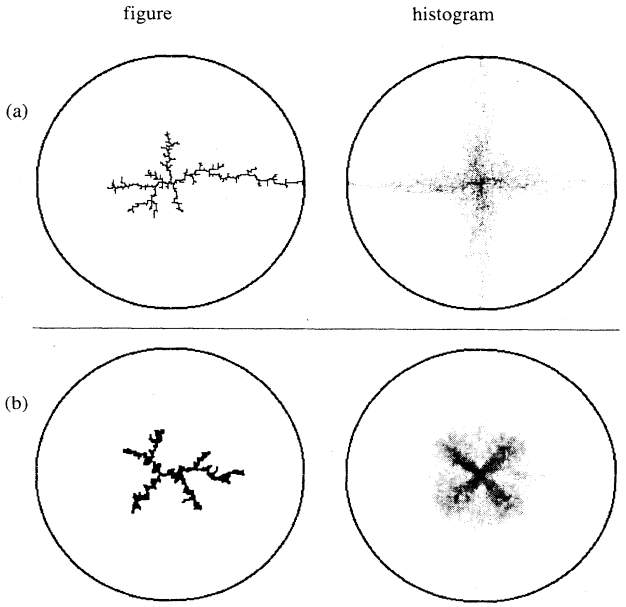

FIG. 7. Results from histogram DLA simulations. The figures on the right are histograms of 100 DLA simulations of 1500 particles each. (a) is a two-hit DLA simulation without sliding, and (b) is a two-hit DLA simulation with sliding. Both (a) and (b) were produced *with erasing* after a new site was added to the crystal. Clearly, the anisotropy seen in Figs. 6(a) and 6(b) is enhanced by this algorithm.

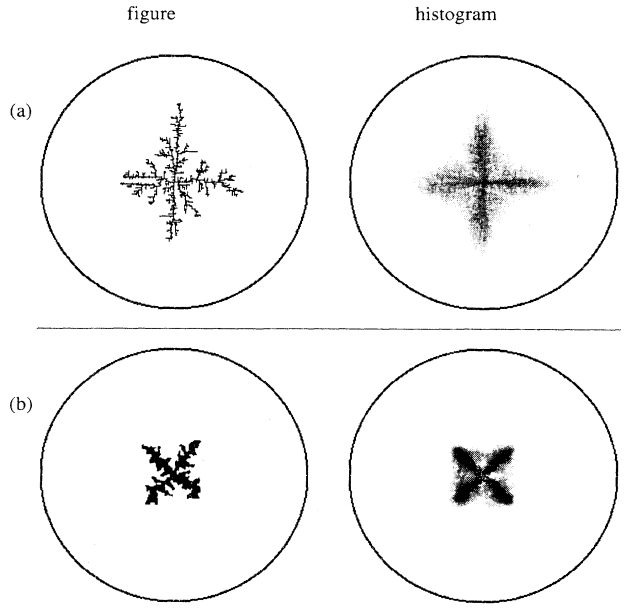

FIG. 8. Results from histogram DLA simulations. These are histograms of 100 DLA simulations of 1500 particles each. (a) is a two-hit DLA simulation without sliding, and (b) is a two-hit DLA simulation with sliding. Both (a) and (b) were produced *without erasing* after a new site was added to the crystal. The anisotropy seen in Figs. 6(a) and 6(b) is enhanced by this algorithm.

and by Ball and Brady for a slightly different "slide" version of DLA [28,37].

As one might predict from the results of Sec. III, the two-hit simulation simply amplified the anisotropy that existed for the one-hit version of the simulation. Regardless of the orientation of the anisotropy, axial for simple DLA and diagonal for one-slide DLA, the two-hit modification amplified the strength of the respective anisotropy.

V. DISCUSSION

We have shown that the probability that a random walker lands on a given site on the boundary of a growth figure can be related to the normal derivative of the solution to Laplace's equation, multiplied by an anisotropic factor $1/f(\theta)$ [see Eq. (2.3)]. The density of landing sites on a train of steps varies as $1/f(\theta)$, where θ is the angle between the normal to the train of steps and the x axis. Hence, the average landing probability for sites on a train of steps is equal to the normal derivative of the solution to Laplace's equation times an anisotropic weighting that corrects for this variation in the density of landing sites.

The escape probability from a train of absorbing steps also varies as $1/f(\theta)$. Thus the escape probability is larger for walkers which have been released from a train of steps oriented in the [1,1] direction than for walkers which have been released from a train which is oriented in the [1,0] direction. This must be considered when one starts walkers from a circular boundary of absorbing sites. An isotropic flux of walkers can be produced if one randomly chooses starting sites on the circular boundary, each with the *same* probability, rather than choosing starting sites with a probability that is proportional to the arc length associated with that site, which is what is frequently done.

We showed that for simple DLA, the average hitting probability, when multiplied by the average growth distance per walker, both of which were found to be anisotropic, gave an isotropic growth rule. This occurs because the average growth distance is proportional to $f(\theta)$.

The cancellation between the anisotropy in the average distance and the anisotropy in the average hitting probability will not occur if one modifies the simulation in a way that changes one of the two factors and not the other. We discussed two-hit DLA with erasing as an example of a typical modification of DLA in which the probabilities of choosing growth sites would be different from those of simple DLA. Relative probabilities of choosing a growth site for any two sites on a given growth figure in a two-hit with erase DLA simulation would spread from their relative probabilities in a simple DLA simulation.

We used a histogramming visualization technique to observe the anisotropy of simple and several modified versions of DLA and found that the multiple-hit simulations, with and without erasing, enhanced any anisotropy that existed in the single-hit version of the simulation. The one-slide simulation, which many believe models crystal growth with surface tension, actually produced figures whose preferred growth directions were along the diagonals, rather than along the axes, as we had found for simple DLA.

In our analysis, we have made several very restrictive assumptions about the way in which the results of a simulation could be related to quantities of interest to us. These assumptions are too restrictive and, for the most part, inappropriate for the analysis of simple DLA simulations. The following four important aspects of the simple DLA simulation separate it from our analysis.

(i) The simulation uses one walker at a time to compute a landing probability.

(ii) The landing probability depends strongly on the *local* environment of a given site.

(iii) The growth at the interface is local.

(iv) The landing probability and the local growth are not stochastically independent.

We consider each of these individually below.

A Monte Carlo simulation can produce the probability of occurrence of a single event by running the simulation a large number of times and observing how often that event occurs. If one wanted to simulate the probability that a random walker lands on site $\mathbf{x}_c$ before landing on other sites on the growing crystal, he or she would allow many walkers to leave from the outer boundary and count the number that land on $\mathbf{x}_c$. Dividing that number by the total number released would give an approximate hitting *probability*. The larger the total number of walkers released, the more accurate the calculation of $D_1(\mathbf{x}_c)$. The simple DLA simulation uses one walker at a time. If one were to interpret this as a calculation of $D_1(\mathbf{x}_c)$, then the probability computed would be 1 for the site that was

hit and zero everywhere else. The statistical error introduced here would be 100%. A simulation which uses a very large number of walkers at each time step to compute $D_1(\mathbf{x}_c)$ would better control the effects of statistical noise on the results.

With this in mind, we attempted to compute actual hitting probabilities from a random walk simulation. We allowed a large number of random walkers to start from a portion of a circle of radius R_2 and to wander in a pie-shaped section towards a portion of a circle located at R_1. Walkers were reflected from the radial boundaries of the pie-shaped wedge. We simply counted the number of walkers that landed on each site. Then we divided that number by the total number released at the outer boundary to get $D_1(\mathbf{x}_c)$. The walkers obeyed the rules on both boundaries that were adopted in the definition of D_1 in Sec. II D. We hoped to verify our expression, Eq. (2.13), for the DLA hitting probability. The results are shown in Fig. 5. We found that the *local* environment of a given site had a much more pronounced effect on the hitting probability (solid squares) than the *overall orientation* of the train of steps. Although the *average* (over 17 neighboring sites) hitting probability for various orientations (open squares) did follow the expected curve, the local environment is clearly dominant in determining the hitting probability. A simulation for which our averaging over a train of steps is appropriate would have to incorporate a smoothing mechanism that would wash out these local effects.

Just as in the local problem discussed above, the growth mechanism in the simple DLA simulation is also plagued with local effects. When we evaluate the normal growth speed for DLA, we assume that a layer of walkers is laid down on the train of steps, and so the entire region is moved normally. In practice, one adds particles one at a time to the surface, not layers of particles. This means that locally there are large differences in the normal growth speed. In other words, a site may move normally one lattice space, while its neighbor may not advance at all. Again, these local effects were not considered in the determination of Eq. (2.14).

Probably the most significant point to be addressed is the correlation between the average hitting probability and the average growth distance, both of which appear in Eq. (2.14). The landing probability and the growth distance in our analysis were treated as stochastically independent variables [39] whose averages we multiplied to obtain an isotropic growth rule. Since fluctuations in the landing probability affect corresponding fluctuations in the growth distance and vice versa, these events are correlated. One cannot multiply their averages to obtain the average of their product. We believe that a clear resolution of this issue is necessary for a complete explanation of the observed anisotropies.

All is not lost. Many smoothing algorithms (some intended to incorporate surface diffusion, capillarity, or interface kinetics) have been suggested as a means of resolving these problems [10,12,29], for example. It is possible that they change the situation in some other way (e.g., introduce capillarity), but they do seem to alleviate some of the statistical noise and might decouple the growth distance and hitting probability. On the other hand, they might introduce poorly understood and unintended biases or anisotropies.

In this paper, we did not address the subject of fractal dimensions or of the scaling laws that are are such an important topic in the literature on the DLA simulations [21–26]. There is similarity of scaling laws and growth morphologies between DLA figures and experimental results. These similarities have been used to support the argument that the simulations bear some resemblance to real crystal growth. In addition, there is excitement in the mathematics community about the simulation's fractal properties and chaotic side-branching. The question that we have addressed here, however, is whether the DLA simulations, as presently implemented, can accurately produce solutions to a particular continuum free boundary problem for field quantities such as energy density and concentration. We believe that it cannot.

ACKNOWLEDGMENTS

This work is supported by the National Science Foundation Division of Materials Science (Grant No. DMR 92-11276). Some calculations were performed at the Pittsburgh Supercomputing Center on the CM2 computer (grant DMR-91-0015P).

[1] T. A. Witten and L. M. Sander, Phys. Rev. Lett. **47**, 1400 (1981).
[2] T. A. Witten and L. M. Sander, Phys. Rev. B **27**, 5686 (1983).
[3] A. Arneodo, Y. Conder, G. Grasseau, V. Hakim, and M. Rabaud, Phys. Rev. Lett. **63**, 984 (1989).
[4] G. Daccord, J. Nittmann, and H. E. Stanley, Phys. Rev. Lett. **56**, 336 (1986).
[5] H. Stanley, Physica A **163**, 334 (1990).
[6] J. F. Fernandez and J. M. Albarran, Phys. Rev. Lett. **64**, 2133 (1990).
[7] J. Nittmann, G. Daccord, and H. E. Stanley, Nature **314**, 141 (1985).
[8] S. Liang, Phys. Rev. A **33**, 2663 (1986).
[9] E. Ben-Jacob, G. Deutscher, N. D. Goldenfeld, and Y. Lareah, Phys. Rev. Lett. **57**, 1903 (1986).
[10] F. Family and T. Vicsek, Comput. Phys. **4**, 44 (1990).
[11] J. Nittmann and H. E. Stanley, J. Phys. A **20**, L981 (1987).
[12] T. Vicsek, Phys. Rev. Lett. **53**, 2281 (1984).
[13] T. Vicsek, Phys. Rev. A **32**, 3084 (1985).
[14] E. Ben-Jacob and P. Garik, Nature **343**, 523 (1990).
[15] P. Wynblatt, J. J. Metois, and J. C.Heyraud, J. Cryst. Growth **102**, 618 (1990).
[16] P. Garik, D. Barkey, E. Ben-Jacob, E. Bochner, N. Broxholm, B. Miller, B. Orr, and R. Zamir, Phys. Rev. Lett. **62**, 2703 (1989).
[17] R. M. Brady and R. C. Ball, Nature **309**, 225 (1984).
[18] E. Ben-Jacob, H. Schmueli, O. Shochet, and A. Tenen-

baum, Physica A **187**, 378 (1992).
[19] H. Fujikawa and M. Matsushita, J. Phys. Soc. Jpn. **58**, 3875 (1989).
[20] H. Fujikawa and M. Matsushita, J. Phys. Soc. Jpn. **60**, 88 (1991).
[21] H. Stanley and N. Ostrowsky, *On Growth and Form: Fractal and Non-Fractal Patterns in Physics* (Martinus, Nijhoff, 1986).
[22] P. Meakin, A. Coniglio, H. E. Stanley, and T. A. Witten, Phys. Rev. A **34**, 3325 (1986).
[23] H. Stanley and P. Meakin, Nature **335**, 405 (1988).
[24] F. Family, Physica A **168**, 561 (1990).
[25] M. Matsushita, K. Honda, H. Toyoki, Y. Hayakawa, and H. Kondo, Phys. Soc. Jpn. **55**, 2618 (1986).
[26] T. Halsey, P. Meakin, and I. Procaccia, Phys. Rev. Lett. **56**, 854 (1986).
[27] P. Meakin, in *Phase Transitions and Critical Phenomena,* edited by C. Domb and J. L. Lebowitz (Academic Press, San Diego, 1988), Chap. 3.
[28] R. C. Ball and R. M. Brady, J. Phys. A **18**, L809 (1985).
[29] R. Xiao, J. I. D. Alexander, and F. Rosenberger, Phys. Rev. A **38**, 2447 (1988).
[30] A. Arneodo, F. Argoul, Y. Couder, and M. Rabaud, Phys. Rev. Lett. **66**, 2332 (1991).
[31] R. Xiao, J. I. D. Alexander, and F. Rosenberger, Phys. Rev. A **39**, 6397 (1989).
[32] R. Xiao, J. I. D. Alexander, and F. Rosenberger, J. Cryst. Growth **100**, 313 (1990).
[33] S. Chandrasekhar, Rev. Mod. Phys. **15**, 1 (1943).
[34] W. W. Mullins and R. F. Sekerka, J. Appl. Phys. **34**, 323 (1963).
[35] F. L. Spitzer, *Principles of Random Walk* (Van Nostrand, Princeton, NJ, 1964).
[36] R. F. Voss, Fractals **1**, 141 (1993).
[37] O.Shonosuke and H. Honjo, Phys. Rev. A **44**, 8425 (1991).
[38] R. Tao, M. A. Novotny, and K. Kaski, Phys. Rev. A **38**, 1019 (1988).
[39] B. V. Gnedenko, *The Theory of Probability* (Chelsea, New York, 1989).

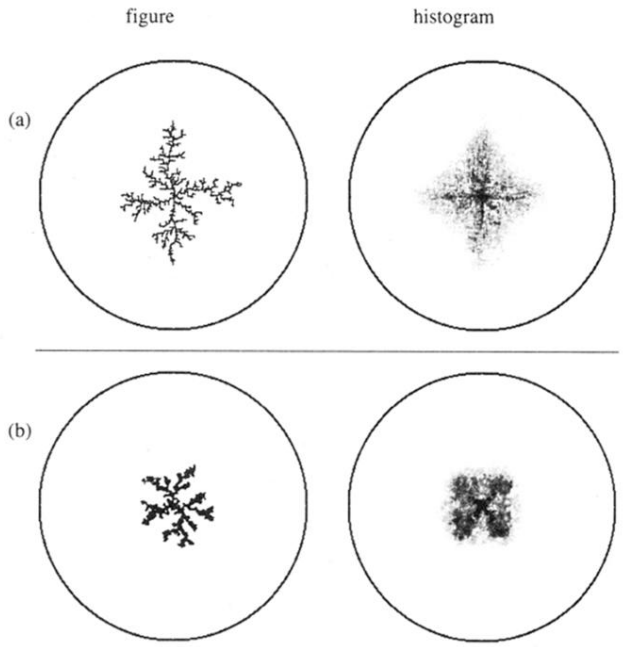

FIG. 6. Results from histogram DLA simulations. The figures on the left are single simulation growth figures of 1500 particles, and the figures on the right are histograms of 100 figures produced by the same algorithm. The shading represents the number of times out of 100 simulations that a growth shape occupied that lattice site. (a) is a simple DLA simulation, and (b) is one-slide DLA. The histograms show a slight anisotropic response to the lattice.

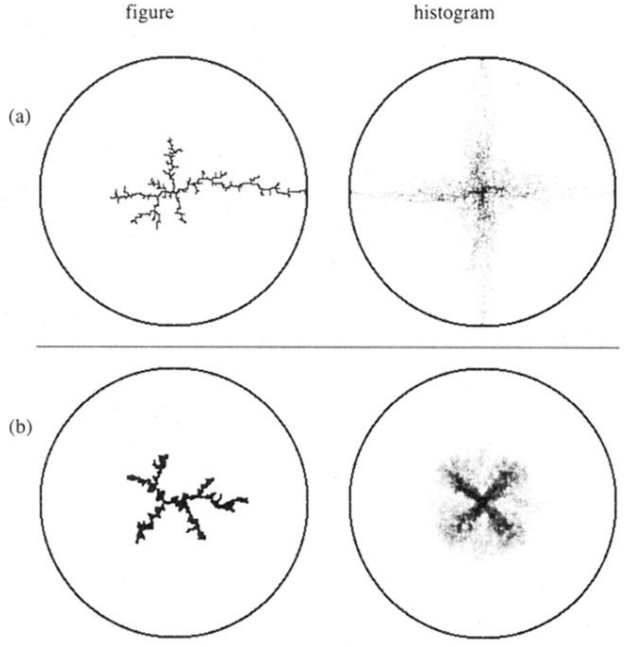

FIG. 7. Results from histogram DLA simulations. The figures on the right are histograms of 100 DLA simulations of 1500 particles each. (a) is a two-hit DLA simulation without sliding, and (b) is a two-hit DLA simulation with sliding. Both (a) and (b) were produced *with erasing* after a new site was added to the crystal. Clearly, the anisotropy seen in Figs. 6(a) and 6(b) is enhanced by this algorithm.

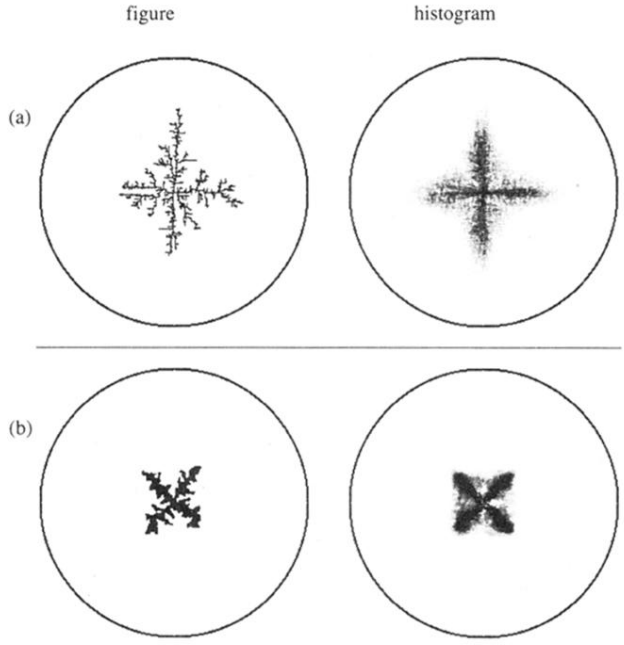

FIG. 8. Results from histogram DLA simulations. These are histograms of 100 DLA simulations of 1500 particles each. (a) is a two-hit DLA simulation without sliding, and (b) is a two-hit DLA simulation with sliding. Both (a) and (b) were produced *without erasing* after a new site was added to the crystal. The anisotropy seen in Figs. 6(a) and 6(b) is enhanced by this algorithm.